THE MICROSTRUCTURAL REPRESENTATION AND FRACTAL NATURE INTEPOLATION ANALYSIS OF FELDSPAR

Dušan M. Milošević[1], Ana Radosavljević-Mihajlović[2], Mimica R. Milošević[3], Nataša G. Đorđević[2], Bojana Marković[4], Mirko Grubisic[2] and Branislav Vlahović[5]

[1]Faculty of Electronic Engineering, University of Nis, 14 Aleksandra Medvedeva 18000 Nis, Serbia;
[1a]Institute of Technical Sciences of SASA, Knez Mihailova 35/IV, 11000 Belgrade, Serbia
[2]Institute for Technology Nuclear and Other Raw Materials,86 Franse d'Epere Blvd. 11000 Belgrade, Serbia;
[3]Faculty of Informatics and Computer Science, Cara Dušana 62-64, University "Union—Nikola Tesla", 11158 Belgrade, Serbia
[4]Faculty of Electronic Engineering, University of Nis, 14 Aleksandra Medvedeva 18000 Niš, Serbia;
[5]North Carolina Central University, USA Durham NC, USA;

Abstract:

This paper presents a comparative analysis of microstructural parameters by the powder X-ray diffraction method on a polycrystalline sample and the fractal analysis. The presented results of microstructural parameters are obtained by crystallographic programs FullProf based on the Rietveld method. The synthetic Ba/Ca-celsian sample has been used for microstructural parameters analysis. The feldspar sample has been synthesized by the thermal induction phase transformation process of ion exchange Ca-LTA zeolite with Ba cation. After the ion exchange Ba/Ca-LTA, the sample was heated at the temperature of 1300°C and the structure of Ba/Ca-feldspar was determined by the X-ray powder diffraction analysis. The X and U shape parameters that contribute to the strain have been reconstructed by fractal interpolation. Once we can reconstruct the shapes, which are quantum mechanics effects, we should provide the data for predicting desired parameters mentioned previously. We reported in this paper the successful application of this advanced and deep microstructure analysis, which confirmed original fractal copies based on the presented morphology characterization.

Keywords: *microstructure; crystallographic software; feldspar; X-ray diffraction analysis; fractal interpolation*

Cooresponding author: a.radosavljevic@itnms.ac.rs

1. Introduction

The microstructural parameters determination is an important part of the ceramic materials characterization process because they determine the crystallite size and micro-strain in the crystal lattice. Those parameters can be designated by using different techniques: transmission electron microscopy (TEM), scanning electron microscopy (SEM) and X-ray diffraction (XRD) [1-4]. Microstructural parameters determine size of the crystallite and microstrain in the crystal lattice. They can be determined using X-ray diffraction analysis, datas based on the broadening of diffraction lines, with so-called line broadening analysis – LBA [5]. According to the literature [6], LBA can be defined as (1) the full width at half maximum (FWHM), which represents the width of the peak at half its maximum intensity, and (2) the integral width β, which is the width of the rectangle that has the same height and surface as the diffraction peak. The most common causes of the line broadening are the presence of small crystallites, structure disorder, presence of dislocations, or microstrain in the crystal lattice.

Rietveld's analysis is one of the most commonly used programs (software) for calculating the size/strain parameters [7]. The software contains modified models for calculating the value of deformation/size based on the anisotropic expansion of diffracted peaks [8, 9]. Two models of size-broadening anisotropy are currently used in Rietveld programs. In the first model proposed by Greaves, the crystal rotation axis is normal to the plate or parallel to the needle axis, and there is no broadening effect. So, only one refined parameter, the plate thickness or the needle diameter, is present [10]. The second model for observing the size-broadening anisotropy is the model of spherical harmonics, proposed by Popa. [11]. Popa and Balzar determined that the apparent crystallites determined in this way (or by conventional methods if available) can be further used in the least-squares refinement program to fit the parameters of a physical model: the shape, orientation, and size distributions of crystallites [12].

By applying this software to X-ray diffraction results, we can refine micro-strain and size parameters, which characterize the examined crystalline materials samples [13, 14]. Furthermore, if we want to predict and design the desired microstructural parameters, we can achieve that goal by applying fractal nature interpolation analysis on the obtained size/micro-strain three-dimensional representation. The crystallographic quantum mechanics analysis is enriched with the fractal interpolating method, which provides the crystallographic sample shape reconstruction, and opens the possibility for micro-structure parameters prognosis and

design [15]. The connection between quantum mechanics and crystallography is very close. Richard Weiss was the first to propose the extraction of quantum mechanical information from crystallographic data [16]. He defined quantum crystallography as a field where crystallographic data are combined with quantum mechanical methods and techniques [17]. Based on the methods of crystallographic quantum mechanics [17] and the determination of crystal structure, we have highly integrated research tools. These methods have an excellent application in modern organic, inorganic, and physical chemistry science. The diffraction and scattering experimental analyses of the atomic-scale structures are necessary for providing quantum mechanics wave functions.

All of the above-mentioned are very important for listed feldspars and other materials. We have innovated some new approaches based on fractal nature analysis, obtained upgraded research and related results, and got advanced desired materials properties. Practically, almost for the first time in crystallographic science and other related and similar research, we have applied fractal interpolation to the three-dimensional representation of the structural parameters of micro deformations/quantities.

The main idea was the reconstruction of microstructure presentations on the mentioned figures. We have made whole new progress in our research to redesign from the points of the figures of the structure, to reach a possible reconstruction. In that sense, we have applied an important novelty based on the fractal interpolation method (Akimo polynomial method) [18] and successfully got excellent results with reconstructed shape structures. We extended our principal idea and research goal towards possibilities that we can, by these quality morphology reconstructions, use as excellent data for prediction and advanced designing of these structures at the very deep and micro-materials crystallographic level. Once we can reconstruct these shapes, we will control the next steps in predicting and designing these required crystallographic properties of the material. In this way, we practically project the expected results in the experiment using compiled crystallographic methods and supporting equipment. We successfully got good results in the reconstruction process with possible neglected minor errors.

The main goals of this work are (a) to determine the crystallite size and microstrain of feldspar by crystallographic programs FullProf; (b) to reconstruct microstructure presentations by the fractal analysis method.

2. Materials and Methods

2.1. Short intro to fractal interpolation

One of the most widely used types of approximation technique is interpolation. It requires the approximation function to pass through predefined points. Suppose, further, that the points $p_i = (x_i, y_i)$, $i = 1, \dots, N + 1$ which we want the interpolation function to pass are given, and that abscissas of these points are arranged in ascending order. In our paper, we have used the Fractal Interpolation Curve (FIC). To obtain the two-dimensional FIC curve, we have used the Iterative Function System (IFS) [19, 20]. IFS are a finite set of contraction mappings $\{w_1, w_2, \dots, w_N\}$ of the complete metric space $(\mathbb{R}^2, d)$ into itself. Let X be a bounded set from $\mathbb{R}^2$, then

$$W(X) = \cup_{i=1}^{N} w_i(X), \tag{1}$$

is Hutchinson operator [21] over $\mathbb{R}^2$. The Hutchinson operator over $\mathbb{R}^2$ is a contraction in metric space $(H(\mathbb{R}^2), h)$, where h is the Hausdorff distance. The fixed point of the Hutchinson operator is IFS attractor. IFS always admits at least one attractor, according to Barnsley [22]. Over points p_i, $i = 1, \dots, n + 1$, we have defined IFS with affine transformations [23-26].

$$w_i \begin{bmatrix} x \\ y \end{bmatrix} = \begin{bmatrix} a_i & 0 \\ c_i & d_i \end{bmatrix} \begin{bmatrix} x \\ y \end{bmatrix} + \begin{bmatrix} e_i \\ f_i \end{bmatrix}, \quad i = 1, \dots, N, \tag{2}$$

and constraints

$$w_i \begin{bmatrix} x_0 \\ y_0 \end{bmatrix} = \begin{bmatrix} x_{i-1} \\ y_{i-1} \end{bmatrix} \text{ and } w_i \begin{bmatrix} x_N \\ y_N \end{bmatrix} = \begin{bmatrix} x_i \\ y_i \end{bmatrix}, \quad i = 1, \dots, N. \tag{3}$$

From equation (2), we can see that every transformation w_i, $i = 1, \dots, N$ has five free parameters a_i, c_i, d_i, e_i and f_i. further, according to equations (3), each transformation has four conditions. So, one parameter in each equation is free. We have selected that the free parameter is d_i. Reason for this choice is in the geometric interpretation of the parameter d_i. Transformation w_i maps the lines parallel y-axes to the lines parallel y-axes. So, a straight line of length l, which is parallel to the y-axis, maps to the straight line $w_i(l)$, which is also parallel to the y-axis. The absolute value of the quotient of the line lengths is equal $|d_i|$.

It is sufficient for the absolute value of the parameter d_i to be less than one to ensure that the affine transformation w_i is a contraction. If all affine transformations w_i, $i = 1, \dots, N$ are contraction, then the IFS attractor is a graph of a continuous function passing

through interpolation points $p_i, i = 1, \dots, N + 1$. This continuous function is the Fractal Interpolation Function (FIF). When the ordinates x_i of the interpolation points $\boldsymbol{p}_i$ are not in ascending order, direct application of IFS, defined by (2) and (3), does not give an interpolation curve that passes through the interpolation points.

In that case we have introduced a reversible transformation

$$T(x_i, y_i) = (u_i, v_i), \qquad i = 1, \dots, N + 1, \tag{4}$$

where

$$u_i = x_0 + \sum_{j=1}^{i}(|x_j - x_{j-1}| + p) = u_{i-1} + (|x_i - x_{i-1}| + c), \qquad v_i = y_{i.} \tag{5}$$

Ordinates u_i are obviously in a strictly ascending order. The positive constant c in (5) is not equal to 0 only when all interpolation points have the same ordinates. In the last step, we have mapped the obtained attractor in (u, v)-plane by inverse transformation

$$T'(u', v') = (x', y'), \tag{6}$$

where

$$x' = x_{i-1} + (x_i - x_{i-1})\frac{u' - u_{i-1}}{u_i - u_{i-1}}, \quad u' \in [u_{i-1}, u_i], \qquad y' = v' \tag{7}$$

back into the (x, y)-plane.

2.2. Samples

For starting material, the zeolite of LTA topology with Ca major extra framework (ratio of Si/Al = 1.00) has used, manufactured by Union Carbide Co [27]. The zeolite precursor of the Ca-LTA topology was ion-exchanged with 0.21M $BaCl_2$ solutions, with a solid/liquid ratio of 1/30. After ion exchange, the modified Ba/Ca-LTA zeolite topology was sintered at a temperature of 1450 ℃ [28]. At this temperature, the zeolite precursor crystallized to mineral celsian, Fig.1. The samples were denoted as Celsian$_{Ba/Ca}$.
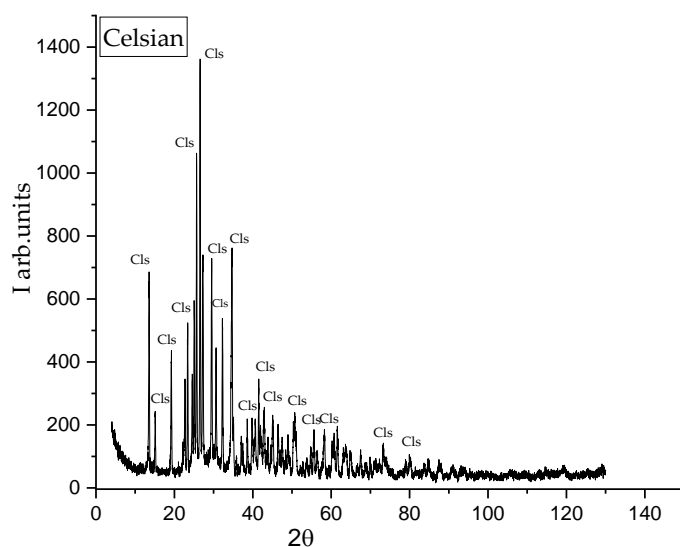
Fig. 1. The X-ray powder diffraction diagram of feldspar sample – Celsian$_{Ba/Ca}$

[JCPDS-74- 1677].

2.3 Methods

The X-ray powder diffraction (XRPD) patterns were obtained on a Philips PW-1710 automated diffractometer Cu Kα operated at 40 kV and 30 mA, with diffracted beam curved graphite monochromatic and a Xe-filled proportional counter. For the Rietveld refinements, data were collected by the step-scanning mode in the range of 4–150° 2θ, count time was increased to 12.5 s, and step size was 0.02°. Structural refinements were performed using the Rietveld method [8] implemented in the FullProf software [14]. The peak profiles were modeled using the Thompson–Cox–Hastings modified pseudo-Voigt (TCH-pV) function. The program Mathematics was used to obtain Fractal Analysis data [29].

3. Results

The basic chemical formula of feldspar is $(M^+M^{2+})[(Si,Al)_4O_8]$, where M^+ and M^{2+} are cations of alkaline and earth alkaline metals. Structurally, feldspars belong to the group of tectosilicates with building units of the chain type, where SiO_4 and AlO_4 tetrahedral are the basic building units [30]. Tetrahedral in the aluminosilicate network are connected in SIJ, which are represented by single four-membered rings (S4R). The

secondary building units are connected in the way that two adjacent tetrahedral are oriented downwards and the other two upwards (Figure 7). Most feldspar crystallizes with an unregulated distribution of Si^{4+} and Al^{3+}, and the process of structure editing itself is quite slow and complicated. Electrostatically, a silicon atom with four positive charges balances four negative charges from 4 oxygen anions.

Most feldspar crystallized with a disordered distribution of Si^{4+} and Al^{3+} in the space group $C2/m$ [31]. The process of the structured ordering into space group $I2/c$ is slow and difficult. During the process of ordering the distribution of the Si/Al cations antiphase domains, a *b*-type can be formed. These domains are inducing a zone–boundary transition from the C (7Å) lattice for disordered feldspars to the I (14Å) lattice for ordered feldspars with the ratio of Al: Si=1:1. The main difference between feldspars is in the number and the intensity of the *b*-type ($h + k = 2n + 1$, $l = 2n + 1$) superstructure reflections. Tribaudino et al. [32] concluded that the *b*-type superstructure reflections in the monoclinic $I2/c$ are due to the displacement of the non-tetrahedral cations. In the data set presented here, the ''*b*'' type reflections were noticed in Celsian$_{Ba/Ca}$, and consequently, the $I2/c$ space group was chosen for refined the structure.

The corresponding Celsian$_{Ba/Ca}$ polymorph structure was refined, starting with structural parameters published in the literature [33]. Based on the structural data, by the X-ray powder diffraction analysis (Fig. 1), the crystal chemical formula was $Ba_{0.84}Ca_{0.13}Al_2Si_2O_8$. The structure was refined in space group $I2/c$ with structural parameters published in the literature (ICSD number 25836, [34]). The structure and profile data refined by the Rietveld method are presented in Tab. I.

Tab. I The structure and Rietveld method for phase profile data refined by $Celsian_{Ba/Ca}$ [28]

	$Celsian_{Ba/Ca}$ $Ba_{0.85}Ca_{0.15}Al_2Si_2O_8$
Space group	*I2/c*
Prof. fun.	Thompson–Cox–Hastings
a (Å)	8.6307 (4)
b (Å)	13.052 (4)
c (Å)	14.401 (4)
β (°)	114.90 (3)
V (Å3)	1471.4 (2)
U	0.09809 (3)
X	0.08111 (3)
Y	0.10451 (3)
Chi2	1.41
R(F)	3.12
R(B)	4.58

To refine the size of the crystallite and micro-strain obtained by XRD, FullProf software [14], based on the Rietveld method [8], was applied. The peak profiles were modeled using the Thompson–Cox–Hastings modified pseudo-Voigt (TCH-pV) function. The crystal structure of feldspar $Celsian_{Ba/Ca}$ [28] refined by the Rietveld method is presented in Tab. II. and Fig. 2. The model of spherical harmonics was used for determination of the crystalline size.

Tab. II Microstructural parameters refined in FullProf crystallographic program, in spherical harmonics model.

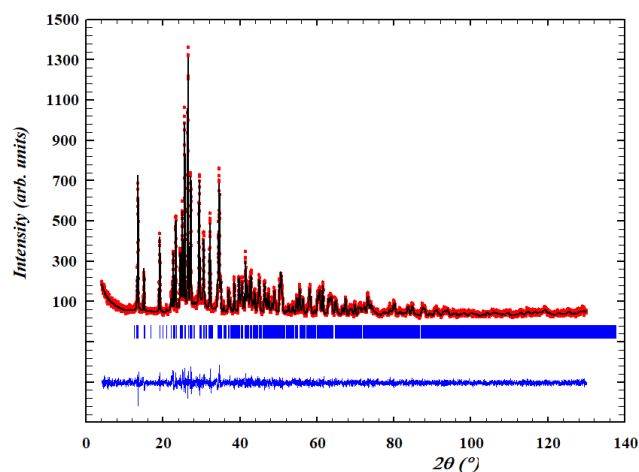|	Celsian$_{Ba/Ca}$
	Ba$_{0.85}$Ca$_{0.15}$Al$_2$Si$_2$O$_8$
Space group	I2/c
Generalized S$_{HKL}$ strain parameters	
S$_{400}$	-0.1065-0.00119
S$_{040}$	-0.0201-0.0
S$_{004}$	-0.0028-0.0012
S$_{220}$	0.0148-0.0148
S$_{202}$	0.1894-0.0113
S$_{022}$	0.0586-0.0068
S$_{121}$	0.0388-0.0164
S$_{301}$	-0.0647-0.0169
S$_{103}$	0.0724-0.0044
average apparent size (Å)	1094 (2)
average mixing strain $\times 10^3$	2.5

Fig. 2. The observed (circles), calculated (continuous line) and difference powder diffraction profiles for Celsian$_{Ba/Ca}$.

3.1. Results and disscusion of the microstructural analysis

The results for microstructural parameters refined in FullProf software in the spherical harmonics model are presented in Table 2. This model is based on the observation that the volume-averaged column length in the Scherrer [5] formula, DV (h), is invariant to the Laue group operations and therefore can be expanded in a series of symmetrized spherical harmonics of polar and azimuthally angles of h, the unit vector along the reciprocal lattice vector H [5]. As is well known, the dhkl spacing between the planes for any reflection is defined by the Miler indexes given by $\sigma^2 (M_{hkl}) = \Sigma\ S_{HKL} h^H k^K l^L$.

It is well known that the width of the diffraction lines, obtained by the Rietveld analysis of diffraction profiles, consists of a convolution of Gaussian and Lorentzian line shapes [35]. The shape parameters X and U (Table 1), which contributions the strain, may duplicate the action of the S_{HKL} parameters [35]. Based on the crystal system, there are certain limitations for the anisotropic strain parameters, which lead to the restrictions on strain parameters presented in Tab. II. The graphic of a three-dimensional representation of microstrain/size microstructural parameters is shown in Fig. 3.
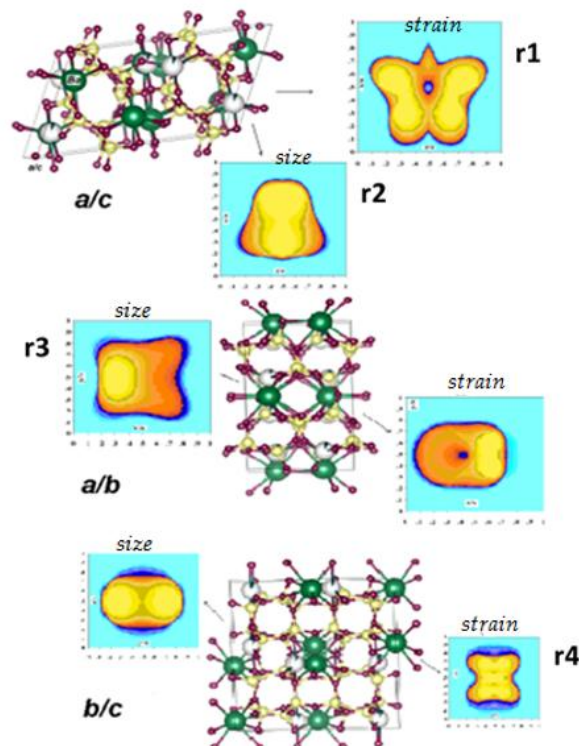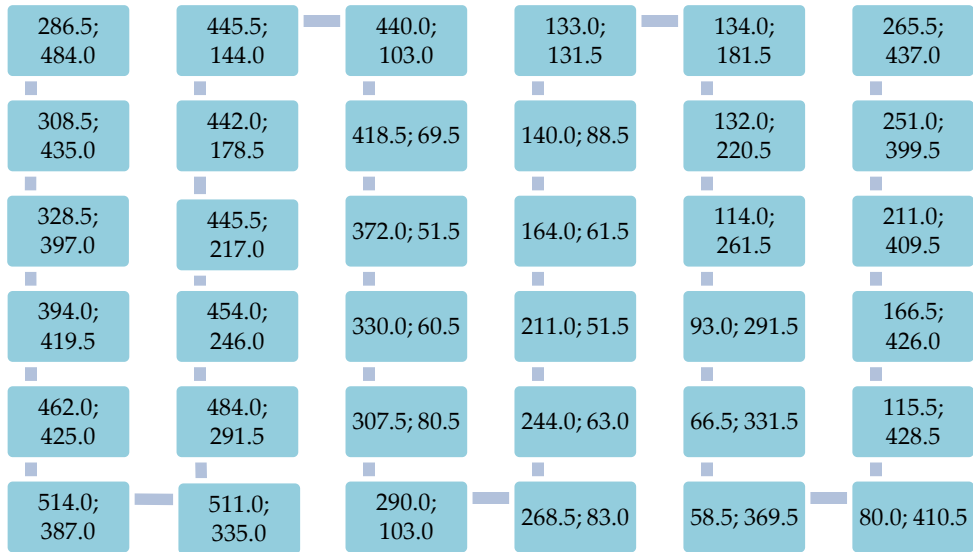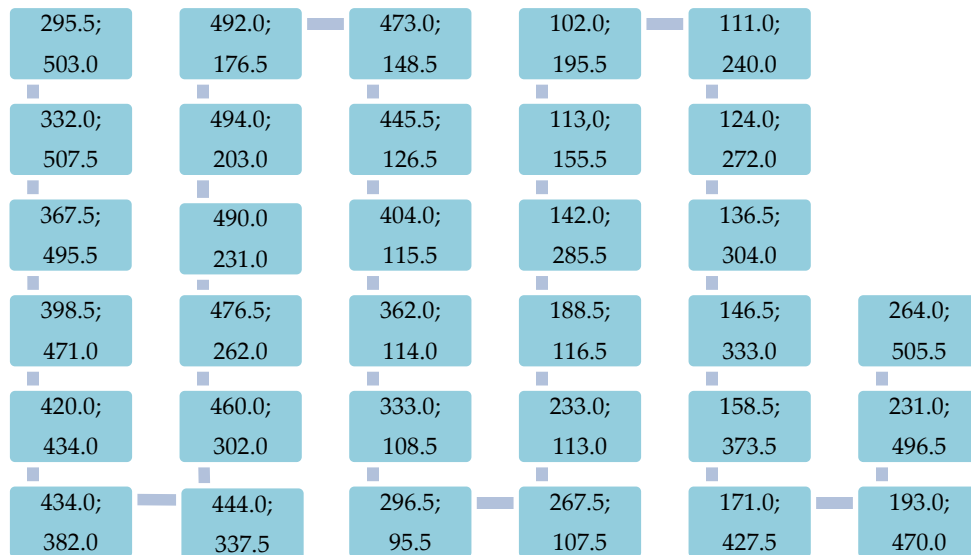

Fig. 3. Size and strain projection in plane *a/b, a/c* and *b/c* for Celsian$_{Ba/Ca}$ three-dimensional representation.
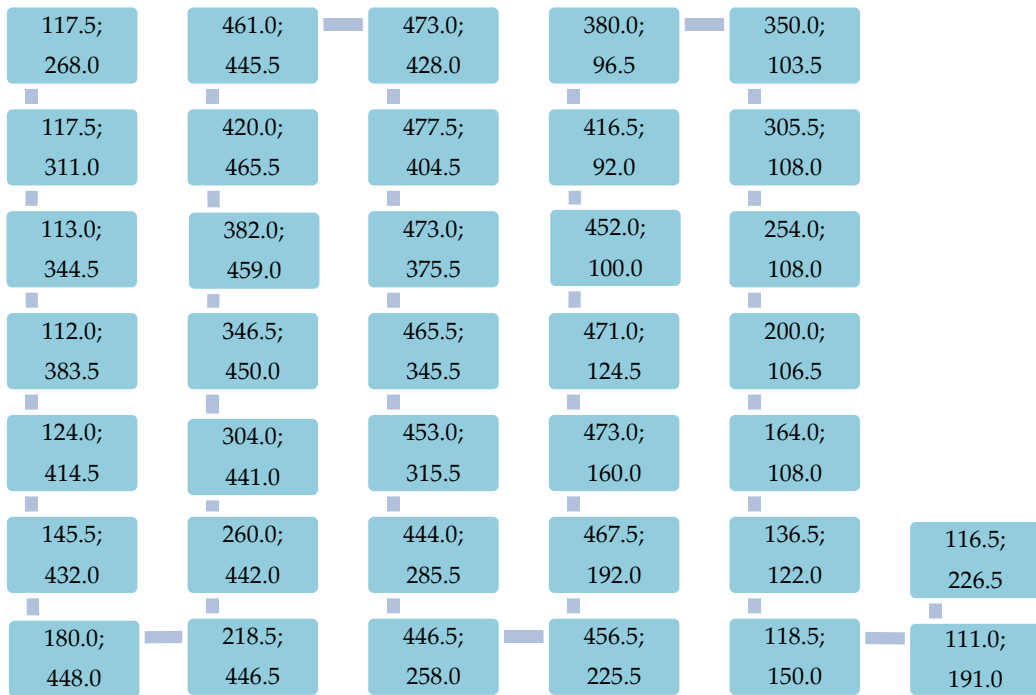
3.2. Fractal interpolation data

From the obtained microstrain/size 3D representations for feldspars crystal structure, we selected four 3D representations (denoted as r1, r2, r3, and r4 in Figure 3) on which we applied the fractal interpolation analysis. The obtained data are taken from Fig. 3 and Tab. I and Tab. II are presented in schemes 1-4.
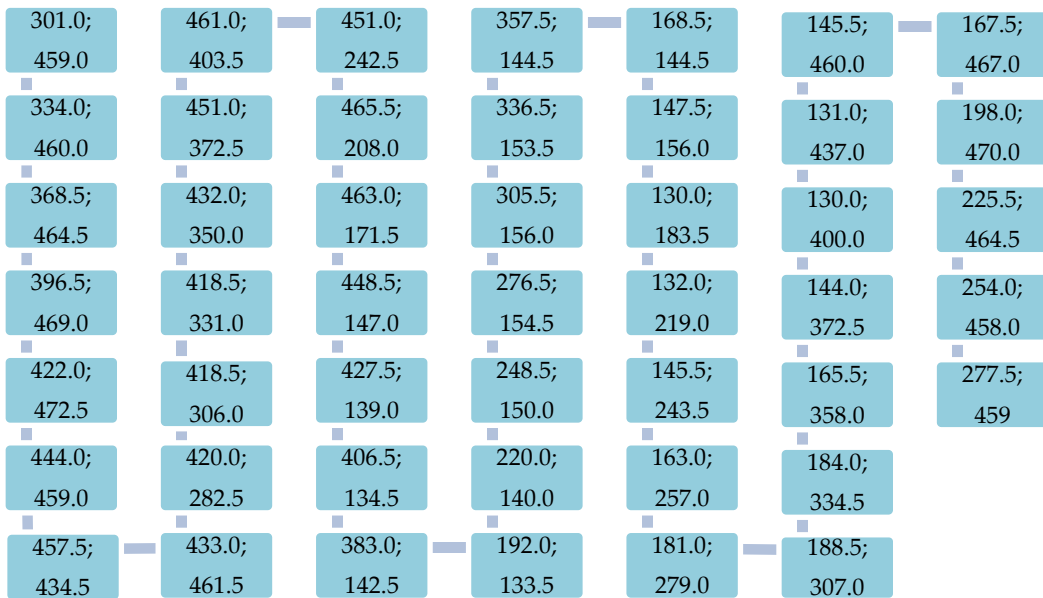
286.5; 484.0	445.5; 144.0	440.0; 103.0	133.0; 131.5	134.0; 181.5	265.5; 437.0
308.5; 435.0	442.0; 178.5	418.5; 69.5	140.0; 88.5	132.0; 220.5	251.0; 399.5
328.5; 397.0	445.5; 217.0	372.0; 51.5	164.0; 61.5	114.0; 261.5	211.0; 409.5
394.0; 419.5	454.0; 246.0	330.0; 60.5	211.0; 51.5	93.0; 291.5	166.5; 426.0
462.0; 425.0	484.0; 291.5	307.5; 80.5	244.0; 63.0	66.5; 331.5	115.5; 428.5
514.0; 387.0	511.0; 335.0	290.0; 103.0	268.5; 83.0	58.5; 369.5	80.0; 410.5

Scheme 1. Fractal interpolation data for 3D representation r1.

295.5; 503.0	492.0; 176.5	473.0; 148.5	102.0; 195.5	111.0; 240.0	
332.0; 507.5	494.0; 203.0	445.5; 126.5	113,0; 155.5	124.0; 272.0	
367.5; 495.5	490.0; 231.0	404.0; 115.5	142.0; 285.5	136.5; 304.0	
398.5; 471.0	476.5; 262.0	362.0; 114.0	188.5; 116.5	146.5; 333.0	264.0; 505.5
420.0; 434.0	460.0; 302.0	333.0; 108.5	233.0; 113.0	158.5; 373.5	231.0; 496.5
434.0; 382.0	444.0; 337.5	296.5; 95.5	267.5; 107.5	171.0; 427.5	193.0; 470.0

Scheme 2. Fractal interpolation data for 3D representation r2.

Scheme 3. Fractal interpolation data for 3D representation r3.

117.5; 268.0	461.0; 445.5	473.0; 428.0	380.0; 96.5	350.0; 103.5	
117.5; 311.0	420.0; 465.5	477.5; 404.5	416.5; 92.0	305.5; 108.0	
113.0; 344.5	382.0; 459.0	473.0; 375.5	452.0; 100.0	254.0; 108.0	
112.0; 383.5	346.5; 450.0	465.5; 345.5	471.0; 124.5	200.0; 106.5	
124.0; 414.5	304.0; 441.0	453.0; 315.5	473.0; 160.0	164.0; 108.0	
145.5; 432.0	260.0; 442.0	444.0; 285.5	467.5; 192.0	136.5; 122.0	116.5; 226.5
180.0; 448.0	218.5; 446.5	446.5; 258.0	456.5; 225.5	118.5; 150.0	111.0; 191.0

Scheme 4. Fractal interpolation data for 3D representation r4.

301.0; 459.0	461.0; 403.5	451.0; 242.5	357.5; 144.5	168.5; 144.5	145.5; 460.0	167.5; 467.0
334.0; 460.0	451.0; 372.5	465.5; 208.0	336.5; 153.5	147.5; 156.0	131.0; 437.0	198.0; 470.0
368.5; 464.5	432.0; 350.0	463.0; 171.5	305.5; 156.0	130.0; 183.5	130.0; 400.0	225.5; 464.5
396.5; 469.0	418.5; 331.0	448.5; 147.0	276.5; 154.5	132.0; 219.0	144.0; 372.5	254.0; 458.0
422.0; 472.5	418.5; 306.0	427.5; 139.0	248.5; 150.0	145.5; 243.5	165.5; 358.0	277.5; 459
444.0; 459.0	420.0; 282.5	406.5; 134.5	220.0; 140.0	163.0; 257.0	184.0; 334.5	
457.5; 434.5	433.0; 461.5	383.0; 142.5	192.0; 133.5	181.0; 279.0	188.5; 307.0	

The main research area in this paper is 3D microstructural characterization on experimental samples Celsian$_{Ba/Ca}$ by two methods. As a part of this experimental research, we got strain projections in the plane as a result of applied characterization methods by the Rietveld method (within FullProf software). As a result of this analysis, we got figures 4. to 7. These microstructure analysis results and presentations are the core point in deep materials crystallographic analysis. These are very important, but we have performed, in our research paper, for the first time in crystallography advanced mathematical-physical methods.

On every Fig. from 4 to 7, we have on the left side original presented structures (r1,…,r4). From these structures, we have taken the data presented in schemes 1 to 4. These data represent interpolation nodes in the method of obtaining fractal interpolation function. As a result of the 3D characterization process, we have reconstructed the shapes of related structures. There is a very high similarity between the experimental and results based on the reconstruction by the fractal interpolation method.
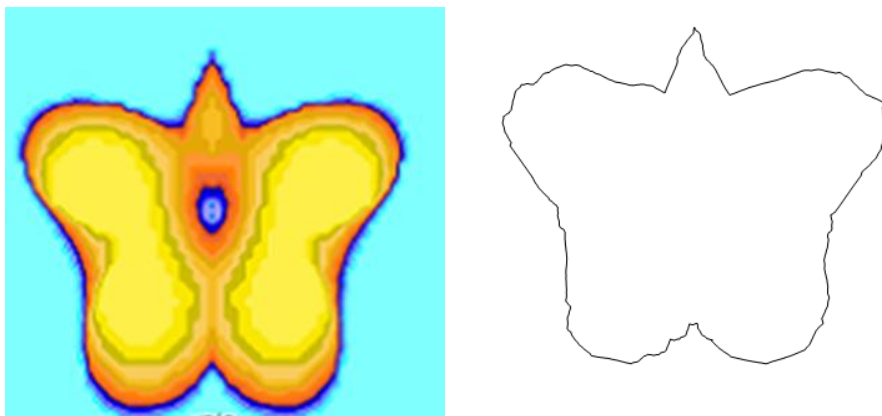
Fig. 4. Strain projection in plane *a/c* for Ba/Cafeld$_{LTA}$ on the left and corresponding fractal interpolation model on the right.
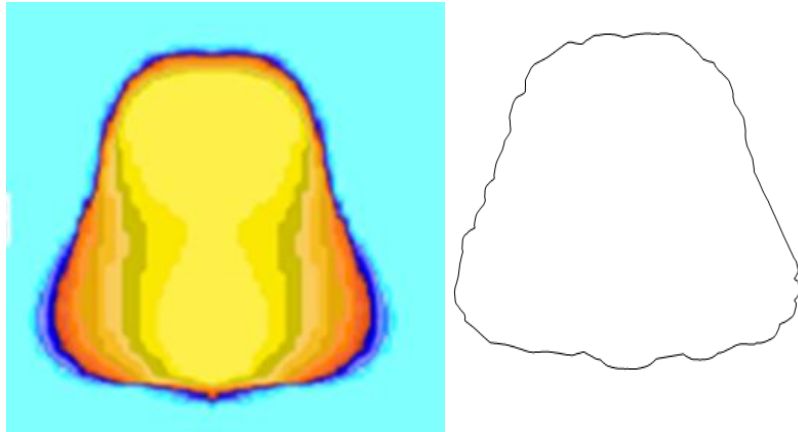
Fig. 5. Size projection in plane *a/c* for Ba/Cafeld$_{LTA}$ on the left and corresponding fractal interpolation model on the right.
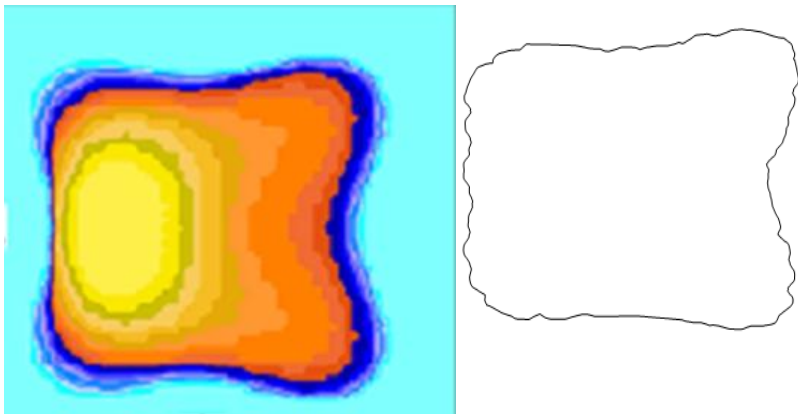
Fig. 6. Size projection in plane *a/b* for Ba/Cafeld$_{LTA}$ on the left and corresponding fractal interpolation model on the right.
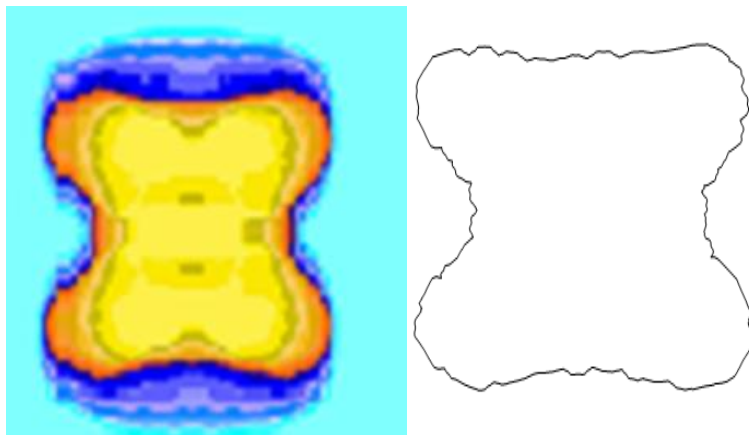

Fig. 7. Strain projection in plane *b/c* for Ba/Cafeld$_{LTA}$ on the left and corresponding fractal interpolation model on the right.

Images from the left side in Fig. 4 - 7 are generally the result of quantum crystallography application analyses [36]. The wave-functions approximation could be improved by the fraction and scattering applied experiments. Charge density models include electron-density distributions, atomic positions, and atomic motion.

4. Conclusions

We have applied, in our research, fractal nature interpolation analysis on the different feldspar size/micro-strain experimental results obtained by crystallographic methods and software to introduce a new characterization and reconstruction approach. It is very significant from the aspect of ceramic materials microstructural parameters determination enhancement, as well as from the aspect of obtaining the predicted and desired crystallite size and micro-strain parameters. Now we can notify the evident very advanced application method novelty within the process of crystallographic characterization. So, in this way, by fractal penetration in crystallographic methods, we opened quite a new frontier for a very high level of improvement and upgrading the experimental results in characterization by mathematical-physical fractal interpolation method applied to clear experimental results and points.

The research has improved by supplementing diffraction experiments, quantum chemically calculated diffraction experiments, and Tailor-made electron densities. The quantum chemistry and diffraction/scattering experiments are integrated as one tool. Our fractal interpolation wave function reconstructions could be treated as an advanced novelty that further develops quantum crystallography analysis methods.

Conflicts of Interest: "The authors declare no conflict of interest."

5. References

1. T. Ungár, J. Gubicza, G. Ribárik, A. Borbéaly, Journal of Applied Crystallography (2001), 34, 298-310.[CrossRef]
2. A. Weibel, R. Bouchet, F. Boulc'h, P. Knauth, Chem. Mater. (2005), 17, 2378–2385. [CrossRef]
3. H.H. Tian, M.M. Atzmon, Philos. Mag. 79 (1998), 8,1769– 1786. [CrossRef]
4. V. Uvarov, I. Popov, Materials Characterization 58 (2007), 883–891.[CrossRef]
5. H.P. Klug, L.E. Alexander, X-ray Diffraction Procedures for Polycristalline and amorphous materials, 2nd edition, John Wiley, Sons, New York 1974.[CrossRef]
6. T. Ungár, Journal of Materials Science 42 (2006), 5, 1584–1593. [CrossRef]
7. A.L. Ortiz, F.L. Cumbrera, F. Sanchez-Bajo, F. Guiberteau, R. Caruso, Journal of the European Ceramic Society 20 (2000) 1845-1851
8. H. M. Rietveld, Acta Crystallographica 22 (1967), 1, 151-152.[CrossRef]
9. J. Rodríguez-Carvajal, M.T. Fernández-Díaz, J.L. Martínez, J. Phys: Condensed Matter 3 (1991), 3215. [CrossRef]
10. A. R. Stokes, A.J.C. Wilson, Proc. Phys. Soc. 56 (1944), 174-181.[CrossRef]
11. A.R. Stokes, Proc. Phys. Soc. 61 (1948), 382-391.[CrossRef]
12. N. C. Popa, Journal of Applied Crystallography 31 (1988), (2), 176–180.[CrossRef]
13. A. Al, Y. Wai Chiang, R.M. Santos, Minerals 12 (2022) 205
14. J. Rodríguez-Carvajal, Commission on Powder Diffraction (IUCr), Newsletter 26 (2001), 12–19.
15. A. Genoni, P. Macchi, Crystals 10 (2020),473.
16. R.J. Weiss, J.J. De Marco, Rev. Mod. Phys. 30,(1958), 59-62.
17. L. Massa, L. Huang, J. Karle, Int. J. Quantum Chem. 56, (1995) 371-384.
18. E. Gordillo-Cruz, J. Alverez-Ramirez, F. Gonzalez, J. Ade los Reyes, Physica A: Statistical Mechanics and its Application 512 (2018), 635-643.[CrossRef]
19. K.R. Tyada, A.K.B. Chand, M. Sajid, Mathematics and Computers in Simulation 190 (2021), 866-891. [CrossRef]
20. A. Gowrisankar, A. Khalili Golmankhaneh, C. Serpa, Fractal Fract. 5 (2021), 157. [CrossRef]
21. J. Hutchinson, Indiana Univ. J. Math. 30 (1981), 713—747.[CrossRef]
22. M.F. Barnsley, Constr. Approx. 2 (1986),303—329.[CrossRef]
23. V. Mitić, G. Lazović, D. Milošević, C.A. Lu, J. Manojlović, S.C. Tsay, S. Kruchinin, B. Vlahović, Modern Physics Letters B, 34 (2020) (19&20), 2040061.[CrossRef]
24. V. Mitić, G. Lazović, D. Milošević, E. Ristanović, S.C. Tsay, M. Milošević, B.Vlahović, Modern Physics Letters B 35 (2021) (4), 2150076.[CrossRef]
25. V. Mitić, G. Lazović, D. Milošević, J. Manojlović, E. Ristanović, D. Simeunović, S.C. Tsay, M. Milošević, M. Soković, B.Vlahović, Brownian motion fractal nature frontiers within the mater, In Bioceramics, Biomimetic and other Compatible Materials Features for Medical Applications. Springer Nature Switzerland AG Gewerbestrasse 11, 6330 Cham, Switzerland, edited by: Stevo Najman, Vojislav Mitić, Thomas Groth, Mike Barbeck, Po-Yu Chen, Ziqi Sun and Branislav Ranđelović (2022), ch. 10, pp. 393--415. *(in press).*

26. V. V. Mitić, D.M. Milošević, B.M Ranđelović, M.R. Milošević, B. Marković, H.J. Fecht, B. Vlahović, International Journal of Modern Physics B, 36 (2022), 4, 2250035. [CrossRef]
27. Ch. Baerlocher, W. Meier, D. H. Olson Atlas of Zeolite Framework TypesStructure Commission of International Zeolite Association, Elsevier, Amsterdam (2001).
28. A. Radosavljević-Mihajlović, M. Prekajski, J. Zagorac, A. Došen, S. Nenadović, Ceramics International, 38, 3 (2012) 2347-2354.
29. P. S. Stanimirović, G. V. Milovanović, Programski paket Mathematica i primena, edicija Monografija, Univerzitet u Nišu, Elektronski fakultet, 2002
30. F. Libau, Structural Chemistry of Silicates, Springer-Verlag, Springer-Verlag Berlin, Heidelberg, New York, Tokyo, edited by Jost, K. 1985. [CrossRef]
31. H. D. Megaw, Acta Crystallographica 9 (1956), 56-60. [CrossRef]
32. M. Tribaudino, P. Benna, Am. Mineral 83 (1998), 83, 159-166.[CrossRef]
33. D.A. Griffen, P.H. Ribbe, Am. Mineral. 61 (1976), 61, 414–418.
34. JCPDS--International Center for Diffraction Data: *Standard X-ray diffraction powder patterns : section 16--data for 86 substances* (Dept. of Commerce, National Bureau of Standards : for sale by the Supt. of Docs., U.S. Govt. Print Off., 1979), also by United States. National Bureau of Standards and Marlene C. Morris (page images at HathiTrust)P. Scherrer, Nachrichten von der Gesellschaft der Wissenschaften, Göttingen, Mathematisch-Physikalische Klasse, 2, (1918) 98–100.[CrossRef]
35. W.P. Stephens, Appl., Cryst. 32 (1999), 281-289.[CrossRef]
36. R. Delhez, T.H. de Keijser, E.J. Mittemeijer, J. Anal. Bioanal Chem. 1982, 312 (1), 1–16.[CrossRef]

Сажетак

У раду је приказана компаративна анализа микроструктурних параметара методом рендгенске дифракције праха на поликристалном узорку и методом фракталне анализе. Приказани резултати микроструктурних параметара добијени су кристалографским програмима ФуллПроф базираним на Ритвелд методи. За анализу микроструктурних параметара коришћен је синтетички узорак Ba/Ca-целзијан. Узорак фелдспата је синтетизован процесом термално индуковане фазне трансформације јонски измењеног Ca-LTA зеолита са катјоном Ba. Након јонске измене Ba/Ca-LTA, узорак је загреван на температури од 1300°C и структура Ba/Ca-фелдспата је одређена анализом рендгенске дифракције праха. Параметри X и U који доприносе напрезању су реконструисани фракталном интерполацијом. Када будемо могли да реконструишемо облике, који су ефекти квантне механике, требало би да обезбедимо податке за предвиђање жељених параметара који су претходно поменути. У овом раду је приказана успешна примена ове напредне и сложене микроструктурне анализе, која је потврдила оригиналне фракталне облике на основу приказане морфолошке карактеризације.

Кључне речи: микроструктура; кристалографски софтвер; фелдспат; Анализа дифракције рендгенских зрака; фрактална интерполација